Multi-Mode Analysis of Scattering by Bodies of Revolutions via the Combined-Field Integral Equation

Multi-mode analysis of scattering by bodies of revolutions via the combined-field integral equation

Fahimeh Sepehripour, Bastiaan P. de Hon, Martijn C. van Beurden, *Senior Member, IEEE*

***Abstract*—The numerical simulation of electromagnetic scattering by PEC bodies of revolution (BORs) involves computing the modal Green functions (MGFs) arising in the electric field integral equation (EFIE) and magnetic field integral equation (EFIE) for a large number of modes. We achieve this by employing five-term recurrence relations that enable the accurate and efficient computation of the MGFs for a large sequence of modes. The computation time of the five-term recurrence relations is decreased by proper truncation of the associated infinite-dimensional matrix representations. The EFIE and MFIE are then employed together in the combined-field integral equation (CFIE), which overcomes the interior resonance problem that occurs in the electromagnetic scattering by PEC BORs with closed geometries. The performance of the proposed technique is validated by analyzing the scattering of modest to large-size PEC bodies of revolution.**

***Index Terms*—Body of revolution, Combined field integral equations, Modal Green function, Recurrence relation.**

I. Introduction

The scattering problem concerning perfectly electric conducting (PEC) objects with axially symmetric geometries has long been of considerable interest in the area of computational electromagnetics [1]–[7]. The scattering by such kinds of symmetric objects, also called bodies of revolution (BORs), are often characterized using integral equations, which are derived based on the boundary conditions applied to the electromagnetic fields at the surface of the BOR. Depending on whether electric or magnetic fields are employed in the formulation, these integral equations can be categorized into two classes: based on the electric field integral equation (EFIE) [8]–[13] and based on the magnetic field integral equation (MFIE) [14]–[19].

Over the past decades, both EFIE and MFIE formulations have been widely used to address electromagnetic scattering by various kinds of PEC BORs with different shapes. Despite the widespread use of these integral equations, application to exterior scattering problems of the EFIE or MFIE on their own is only valid at frequencies for which the respective integral equation has no interior resonance. In fact, at the resonance frequencies, the respective EFIE or MFIE break down due to the presence of non-unique (source-free) solutions, rendering them inaccurate.

One approach to overcome the internal resonance problem of the MFIE and EFIE for external scattering problems is to combine them such that the boundary conditions at the surface of the BOR are imposed for both electric and magnetic fields simultaneously. This hybrid formulation, known as the combined field integral equation (CFIE), has been proven effective [20]–[23], and is known to resolve the resonance problem of the EFIE and MFIE. Yet, the computation of the corresponding integral equation kernels, known as the modal Green functions (MGFs), can be a challenge. Of course, the MGFs corresponding to both EFIE and MFIE become singular when the source and observation points get close to each other [24]–[26]. This singular behavior severely affects the speed and accuracy of the computation, especially when computing the MGFs for many modes. The computation of such integrals can be accomplished by singularity extraction methods. In this approach, the MGF is solved by separating it from the entire MGF and handling it individually. Despite its applicability, the decomposition of the MGF into separate components handled by separate algorithms is less elegant in problems in which many modes contribute, such as the scattering by large PEC BORs impinged by an obliquely incident plane wave.

Recently, we proposed an efficient approach for computing the full EFIE MGF including its singular part, in which the MGF is computed based on a five-term recurrence relation in a direct manner without separating the MGF into singular and regular parts [27]. The computation via the five-term recurrence relation was accomplished in a stable manner by performing the LU decomposition of the associated penta-diagonal matrix. This reduces the computational complexity. While the direct nature of such an approach is favourable for scattering problems that involve many modes, its applicability is still restricted by the interior resonance problem mentioned before, unless it is used in a combined manner together with its MFIE counterpart.

Below, we provide the MFIE counterpart of the EFIE five-term recurrence relation, and cast both in a single unified form. We shall also demonstrate that the computation times of the corresponding matrix form representations for both the EFIE and MFIE five-term recurrence relations can be reduced significantly through proper truncation of the infinite-dimensional matrix systems. Then, we combine the EFIE and MFIE formulations to construct the CFIE to overcome the interior resonance problem of PEC BORs for closed geometries. We demonstrate the accuracy and efficiency of the CFIE method through scattering examples for modest to large-size PEC BORs of various shapes. For the modest cases, we compare the results with those available in the literature. Not only does this paper offer a direct solution for the computation of the modal Green functions (distinct from the singularity extraction methods [7], [19], [26]), but also it extends the EFIE

The authors are with the Department of Electrical Engineering, Eindhoven University of Technology, Eindhoven 5600 MB, The Netherlands (e-mail: f.sepehripour@tue.nl;b.p.d.hon@tue.nl; m.c.v.beurden@tue.nl.

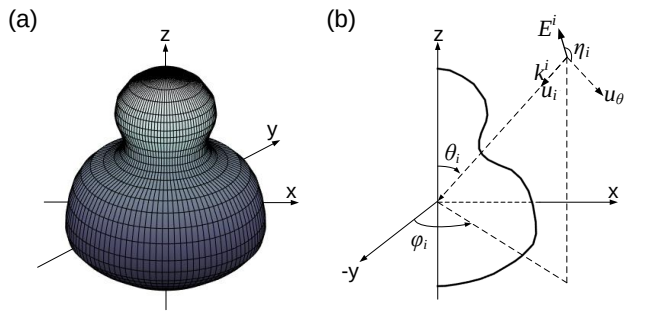

Fig. 1. (a) An axially symmetric PEC object (BOR) with an arbitrary shape, (b) Corresponding generating curve of the BOR. By rotating the generating curve along the axis of symmetry, the full geometry of the BOR is obtained.

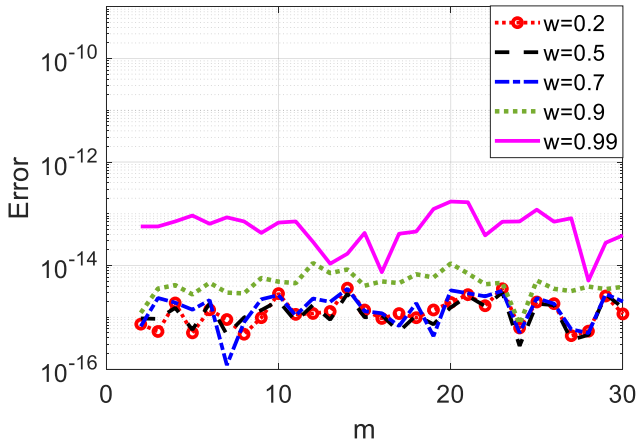

Fig. 2. Error of the computation of $g_m^H(w)$ as a function of the mode index m. The error is computed for various values of w, for $k_0 = 2\pi$, $\rho = \rho' = 0.25$, using the penta-diagonal matrix approach described in Appendix A.

recurrence relation in [27] to the MFIE case with an enhanced computational speed.

The paper is organized as follows. In Section II, the five-term recurrence relations for computing the MGFs arising in the EFIE and MFIE are discussed. Section III discusses the reduction of computation times as a consequence of proper truncation of the corresponding infinite-dimensional penta-diagonal matrices. The EFIE and MFIE formulations are then employed in Section IV in the combined-field formulation (CFIE) to evaluate the scattering by PEC BORs with closed geometries for an incident plane wave. The accuracy of the proposed method is validated by analyzing the scattering of modest to large-size PEC BORs.

II. CFIE FOR BODIES OF REVOLUTION

Consider the arbitrarily-shaped PEC BOR shown in Fig. 1(a), illuminated by an incident plane wave with the parameters θ_i and ϕ_i to describe the angle of incidence. The BOR is placed in free space. Owing to the axial symmetry of the BOR, the electromagnetic scattering from the BOR can be characterized using its generating curve. Its rotation along the radial axis produces the three-dimensional geometry of the BOR, see Fig. 1(b). After discretization of the pertaining integral equations, the associated discretized version of the combined field integral equation is expressed as

$$\left[(1-\beta)\mathbf{Z}_{MFIE}+\frac{\beta}{\eta_0}\mathbf{Z}_{EFIE}\right]\mathbf{J}_s = (1-\beta)\mathbf{V}_{MFIE}+\frac{\beta}{\eta_0}\mathbf{V}_{EFIE} \tag{1}$$

in which $\mathbf{Z}_{MFIE}$ and $\mathbf{Z}_{EFIE}$ are the MFIE and EFIE impedance matrices, and $\mathbf{V}_{MFIE}$ and $\mathbf{V}_{EFIE}$ are the corresponding excitation vectors. Further, η_0 is the free-space intrinsic impedance and $0 < \beta < 1$ is the combination factor of the CFIE. The kernels of $\mathbf{Z}_{MFIE}$ and $\mathbf{Z}_{EFIE}$ are known as the modal Green functions, corresponding to the MFIE and the EFIE, respectively. For the MFIE and EFIE, the MGFs are given by [1], [19], [26]

$$\begin{aligned} g_m^H &= \int_0^\pi \cos(m\alpha)(1+jk_0R(\alpha))\frac{e^{-jk_0R(\alpha)}}{R^3(\alpha)}d\alpha, \\ g_m^E &= \int_0^\pi \cos(m\alpha)\frac{e^{-jk_0R(\alpha)}}{R(\alpha)}d\alpha, \end{aligned} \tag{2}$$

where $R(\alpha) = \sqrt{\rho^2+\rho'^2-2\rho\rho'\cos\alpha+(z-z')^2}$ is the distance between the source point (ρ',z',ϕ') and observation point (ρ,z,ϕ), and $\alpha = \phi - \phi'$. Additionally, k_0 denotes the free-space wavenumber and m is the Fourier mode index in the azimuthal direction. The numerical computation of these MGFs requires special attention. For the EFIE case, a direct method based on a five-term recurrence relation, by which the corresponding MGF can be accurately computed in a stable manner was proposed in [27]. In the following, we introduce a five-term recurrence relation that also accounts for the direct computation of the MGF arising in the MFIE.

A. Five-term recurrence relation for computing the MGF arising in the EFIE and MFIE

By following a procedure similar to the one proposed in [27], one can obtain a five-term recurrence relation for the direct computation of the MGF of the MFIE method. This relation is derived in Appendix A. The following formula summarizes the associated recurrence relations for the MGFs of both MFIE and EFIE:

$$\begin{aligned} &\left(\frac{wk'^2}{16(m-1)(m+1)}+\frac{w-2}{w}\right)g_m = \frac{wk'^2}{32m(m-1)}g_{m-2} \\ &-(\frac{1}{2}-\frac{s}{4m})g_{m-1}-(\frac{1}{2}+\frac{s}{4m})g_{m+1}+\frac{wk'^2}{32m(m+1)}g_{m+2}, \end{aligned} \tag{3}$$

where $s = 1$ corresponds to the EFIE (g_m^E) and $s = -1$ corresponds to the MFIE (g_m^H). The parameter $w = 4\rho\rho'/((\rho+\rho')^2+(z-z')^2)$ is the transformation variable and $k' = 2k_0\sqrt{\rho\rho'/w}$. The benefits of the proposed recurrence relation have been demonstrated in [27] for the EFIE. The MFIE is analyzed below in the context of the recurrence relation cast as a penta-diagonal matrix system centered around the main diagonal. To this end, the infinite penta-diagonal matrix is truncated to a finite $M \times M$ matrix, in which the truncation number M depends on the maximum mode number taken into account to solve the sequence of integral equations as well

as the values of w. The resulting finite-dimensional matrix system can then be solved in a fast and stable manner, based on the same arguments as provided in [27]. Fig. 2 represents the associated computational error for g_m^H as a function of m for various values of $w \leq 0.99$. The reference was computed using Mathematica's `NIntegrate` method with the accuracy goal of 16 digits. Furthermore, in the computation, the penta-diagonal matrix was truncated at $M = 100$ and the initial values g_0^H and g_1^H were computed with an accuracy of 10^{-15} with Matlab's integration routine `integral`. The integration for the computation of initial values required for the recurrence relation is performed using floating point with double precision. The absolute error tolerance of the integration was set to 1E-15 to achieve 15 decimal places of accuracy. As observed, the error level is comparable to machine precision (10^{-15}) for the first 30 modes, verifying the accuracy and stability of the proposed recurrence relation. Together with the EFIE recurrence relation proposed in [27], the MFIE recurrence relation derived here enables the direct computation of the MGFs arising in the CFIE.

III. Acceleration of the MGF scheme for $w \to 1$

The computation of the modal Green functions only becomes tractable upon truncating the recurrence relation after a finite number of steps, i.e., the truncation number M for the penta-diagonal matrix. This is due to the fact that the system is solved as a penta-diagonal matrix and not as a forward recurrence, since the latter is unstable. The five-term recurrence relation is fourth-order and hence admits four sequences, distinguished through initial (or boundary) conditions. In the forward direction, the right solution that satisfies the right initial conditions is dominated by one or more wrong sequences that show exponential growth relative to the right one and are excited due to round-off error. In a practical situation, the number of modes that need to be taken into account in solving the sequence of integral equations is truncated to mode N, implying that g_N is still needed to sufficient accuracy and any subsequent values g_{N+n}, $n \leq 1$, are of no interest. The relation $k\rho_{max}sin(\theta) + 6$ provides a rough estimation for the minimum number of modes to ensure sufficient accuracy for a plane-wave excitation, which is the assumption used in the entire paper [1], [26]. To obtain the sequence g_2 to g_N with sufficient accuracy, the truncation number M of the penta-diagonal matrix must exceed the value N, i.e. $M > N$. However, an additional constraint applies to the truncation number M that involves the accuracy with which the sequence g_2 to g_N is obtained. To demonstrate how the truncation number M is influenced by the parameter w, we perform a numerical experiment by computing the absolute error in the MGFs g_3^H and g_3^E, i.e. for the fixed mode $m = 3$, for various values of w and for an increasing truncation number M. The computation was performed in the same way as for Fig. 2 and the result is shown in Fig. 3. It is readily observed that the behavior of the error for the MFIE and EFIE is quite similar. More importantly, we observe that the error converges exponentially, but the rate of convergence becomes slower when w approaches 1. To maintain a fixed

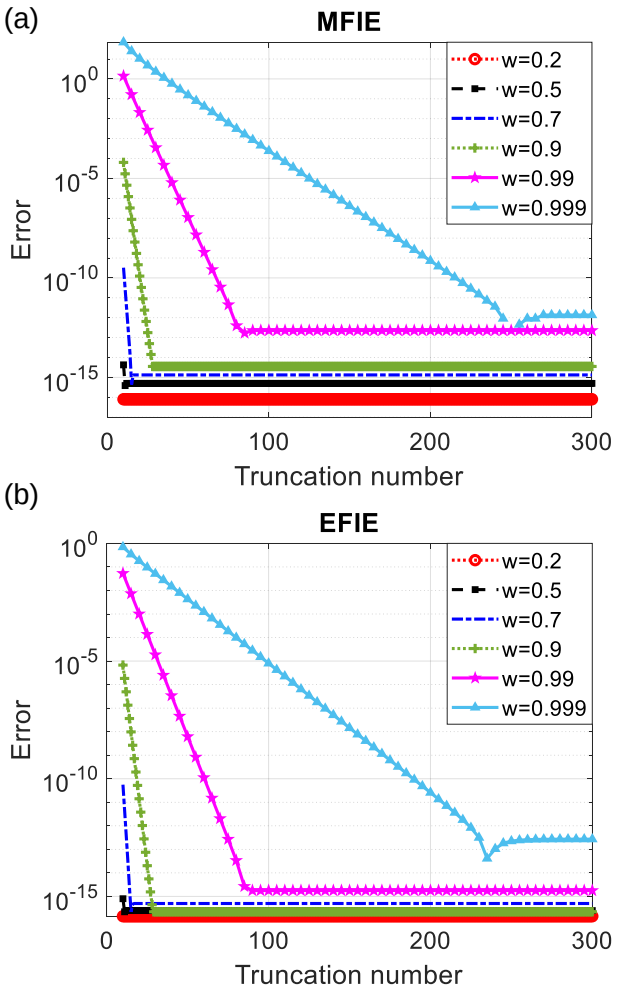

Fig. 3. Absolute error in g_3 for various values of w, with $k_0 = 2\pi$, $\rho = 0.25$ and $\rho' = 0.25$, as a function of the truncation number M. (a) MFIE and (b) EFIE.

level of accuracy in the MGFs up to a certain mode number, the truncation number M needs to be much larger for $w \to 1$ as compared to cases where w is significantly smaller than 1.

This observation can also be explained by the concept of degrees of freedom and rank deficiency, as discussed in [28]–[32]. More specifically, small values of w correspond to a highly rank-deficient interaction between source and observer, allowing one to use fewer modes for the computation. On the other hand, for w close to 1, the source and observer almost overlap, leading to no rank deficiency and implying that many modes are required for the analysis.

For further evaluation, we performed an analysis to examine the change in the truncation number (M) as a function of w. To this end, for each value of w, the truncation number was swept to find the minimum value required to achieve the prescribed error. The results of this investigation are presented in Fig. 4. As observed in this figure, for the case under investigation, the truncation number M scales almost reciprocally with $(1-w)$, i.e. $M \propto (1-w)^{-0.5}$ indicated by the solid red curve in the figure.

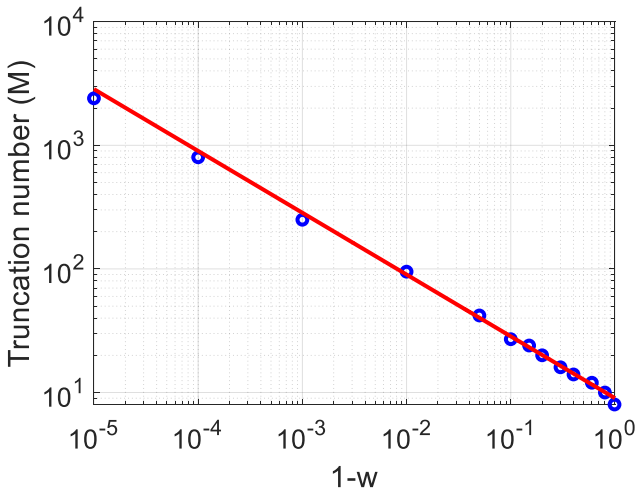

Fig. 4. Variation of the truncation number (M) as a function of $1-w$. The truncation number M scales almost reciprocally with $1-w$, i.e. $M \propto (1-w)^{-0.5}$ (the solid red curve in the figure plots this relation).

Increasing the truncation number increases the computation time. To overcome the increase in the truncation number M and the associated increase in computation time for w close to 1, the sequence of MGFs can alternatively be computed from the recurrence relation by also providing the end values of the recurrence relation, leaving the MGFs to be computed for the intermediate modes. Hence, if we need g_0 to g_N, then we can compute g_0, g_1, g_{N-1}, and g_N, e.g. via numerical quadrature, and compute the intermediate MGFs $g_2, \ldots, g_{N-2}$ via the five-term recurrence relation in the form of the associated penta-diagonal matrix. In this way, we only make an approximation in computing the initial and end values of the sequence of MGFs and no truncation error is introduced. This is of course at the expense of computing the extra values g_{N-1}, and g_N. The resulting linear system is given by

$$C \begin{bmatrix} g_2 \\ g_3 \\ g_4 \\ g_5 \\ \vdots \\ g_{N-3} \\ g_{N-2} \end{bmatrix} = \begin{bmatrix} -a_2 g_0 - b_2 g_1 \\ -a_3 g_1 \\ 0 \\ 0 \\ \vdots \\ -e_{N-3} g_{N-1} \\ -d_{N-2} g_{N-1} - e_{N-2} g_N \end{bmatrix}, \tag{4}$$

The matrix C is written in the following form

$$C = \begin{bmatrix} c_2 & d_2 & e_2 & 0 & 0 & \cdots \\ b_3 & c_3 & d_3 & e_3 & 0 & \ddots \\ a_4 & b_4 & c_4 & d_4 & e_4 & \ddots \\ \vdots & \ddots & \ddots & \ddots & \ddots & \ddots \\ 0 & \cdots & a_{N-3} & b_{N-3} & c_{N-3} & d_{N-3} \\ 0 & \cdots & \cdots & a_{N-2} & b_{N-2} & c_{N-2} \end{bmatrix}, \tag{5}$$

TABLE I
COMPUTATION TIMES FOR THE MGFS ARISING IN THE EFIE AND MFIE FOR MODES 0 TO 20, FOR DIFFERENT VALUES OF w AND FOR THE TWO METHODS DISCUSSED IN THE MAIN TEXT. ADDITIONAL PARAMETERS: $k_0 = 2\pi$, $\rho = 0.25$, $\rho' = 0.25$.

w	M method I	EFIE method I (sec)	EFIE method II (sec)	MFIE method I (sec)	MFIE method II (sec)
0.5	13	0.05	0.07	0.06	0.08
0.9	27	0.05	0.07	0.06	0.077
0.99	100	0.06	0.06	0.063	0.064
0.999	250	0.075	0.06	0.1	0.08
0.9999	800	0.3	0.09	0.36	0.09
0.99999	2400	3.6	0.2	3.7	0.21
0.999999	5800	28	0.8	31	0.9

in which

$$\begin{aligned} a_n &= -\frac{wk'^2}{32n(n-1)}, \qquad b_n = (\frac{1}{2} - \frac{s}{4n}), \\ c_n &= \frac{w-2}{w} + \frac{wk'^2}{16(n-1)(n+1)}, \\ d_n &= (\frac{1}{2} + \frac{s}{4n}), \qquad e_n = -\frac{wk'^2}{32n(n+1)}. \end{aligned} \tag{6}$$

To see when this approach is computationally expedient, we compare the performance in terms of computation time for the two methods, i.e. truncating the infinite matrix at matrix dimension M and computing g_0 and g_1 only (method I) and truncating the recurrence relation after mode N and compute g_0, g_1, g_{N-1} and g_N (method II). Table I presents the computation time of the MGFs arising in the EFIE and MFIE for $N = 20$ modes. For method I, the truncation number M corresponding to each value of w is mentioned in the second column of the table, which is chosen in a way to guarantee that the absolute error is below 10^{-15}. The computation of the initial values g_0, g_1, g_{N-1}, and g_N is performed by Matlab's `integral` routine. As observed from the table, for $w > 0.99$ the computation times of method II are equal or smaller than those of method I. For $w \leq 0.99$, on the other hand, method I is more efficient in terms of computation time. As a result, in the remaining of this paper, method I is employed for $w \leq 0.99$. For $w > 0.99$, method II is employed to reduce the computation time when w approaches 1.

IV. NUMERICAL RESULTS

Resonances are ubiquitous in many electromagnetic problems. The interior resonances occurring in the scattering problems that involve PEC objects with closed geometries may render the solution of the EFIE or MFIE inaccurate and unstable. When the EFIE and MFIE are combined with each other properly (i.e. CFIE), the resonance problem can be resolved. Below, the accuracy and computation time of the proposed method are investigated for BORs of different sizes.

In all of the numerical results discussed below, the combination factor of the CFIE is chosen as $\beta = 0.5$. Furthermore, for solving the associated integral equations, the method of

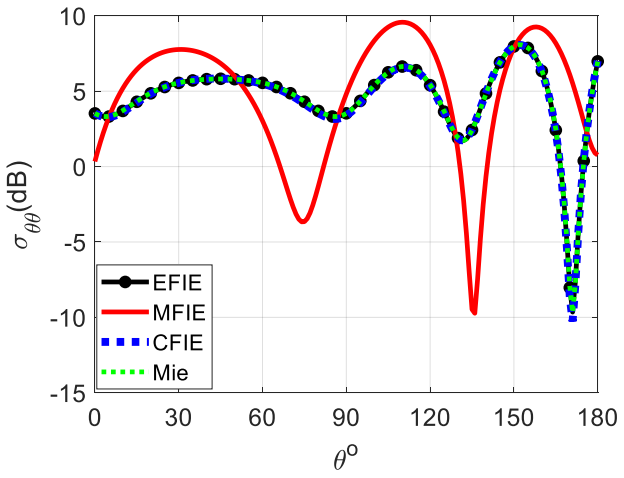

Fig. 5. Investigation of the interior resonance behavior through the $\theta\theta$ component of the bistatic radar cross-section at the plane $\phi_{obs} = 0$ at the frequnecy of 237.3 MHz. The results are obtained using the proposed CFIE (dashed blue), EFIE (dashed black), and MFIE (solid red) methods, and compared with Mie series [33] (dashed Green). The maximum deviation between CFIE technique and the Mie series is 0.7 dB.

moments with Galerkin discretization has been employed. To this end, the surface currents over the generating curves are discretized with piece-wise constant and piece-wise linear functions in the ϕ direction and the direction tangential to the generating curve, respectively. Other technical details regarding the implementation of the EFIE and MFIE, and the handling of singularities in the corresponding MGFs can be found in [12], [19].

A. Evaluating interior resonance behavior

To illustrate the interior resonance problem, let us consider a PEC sphere with radius r, placed in free space. The internal resonance frequencies of such a scatterer can be found analytically from the zeros of the following expressions [34]–[36]

$$A_n = -\frac{(k_0 r j_n(k_0 r))'}{(k_0 r h_n(k_0 r))'}, \qquad B_n = -\frac{j_n(k_0 r)}{h_n(k_0 r)}, \tag{7}$$

where A_n and B_n correspond to TM (electric) and TE (magnetic) resonance functionals, respectively, and the prime denotes the derivative with respect $k_0 r$. Further, j_n and h_n are the spherical Bessel and Hankel functions of the first kind, and k_0 is the wavenumber of the background medium. For a sphere with radius $r = 1\,\mathrm{m}$, we employ both the EFIE and MFIE to evaluate the corresponding bistatic radar cross-section (RCS) near one of the interior resonance frequencies, namely $f = 237.3$ MHz, obtained by setting $A_3 = 0$, corresponding to TM_{31}^{int}. The incident polar angle is set to $\theta_i = \pi/4$. The generating curve of the spherical BOR is discretized into 40 segments and Fourier modes $m = -15, \ldots, 15$ are taken into account for the computation. Fig. 5 represents the bistatic radar cross-section $\sigma_{\theta\theta}$, which is the co-polarized component

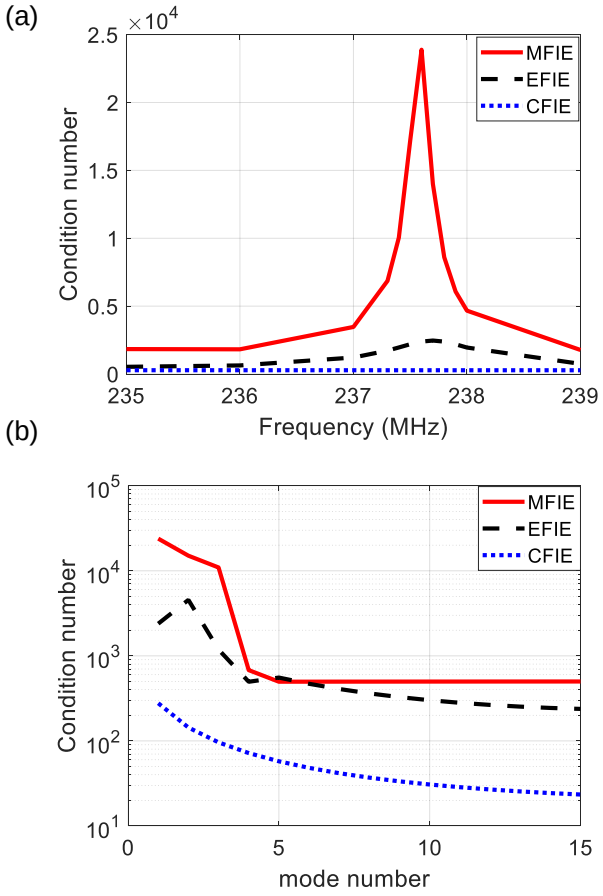

Fig. 6. Evaluating interior resonance behavior. (a) Condition numbers of different formulations around the resonance frequency for mode $m = 1$. (b) Condition numbers of different formulations as a function of Fourier mode at 237.6 MHz.

of the 2×2 RCS matrix for a θ-polarized incident plane wave. The analytical solution obtained from the Mie series is also plotted for comparison. As observed, the MFIE solution (red line) is inaccurate around the resonance frequency under investigation. By employing the CFIE formulation (dashed blue line), however, the inaccuracy is avoided. In particular, the maximum deviation between the CFIE technique and the Mie series is 0.7 dB in this figure.

For further assessment, we also provide the condition number of the impedance matrices associated with the EFIE, MFIE, and CFIE. Fig. 6(a) shows the corresponding condition numbers around the resonance frequency for mode $m = 1$. As can be observed from this figure, both the EFIE and the MFIE lead to a high condition number near the resonance. However, the CFIE represents a flat behavior, indicating its stability. It should be mentioned that the peak value of the condition number for both EFIE and MFIE occurs at $f = 237.6$ MHz, which is a bit larger than the resonance frequency ($f = 237.3$ MHz). This is due to the inscribed discretization of the sphere under investigation. Fig. 6(b), plots the condition numbers of the various integral operators as a function of the mode index at $f = 237.6$ MHz. A similar behavior as Fig. 6(a) is observed.

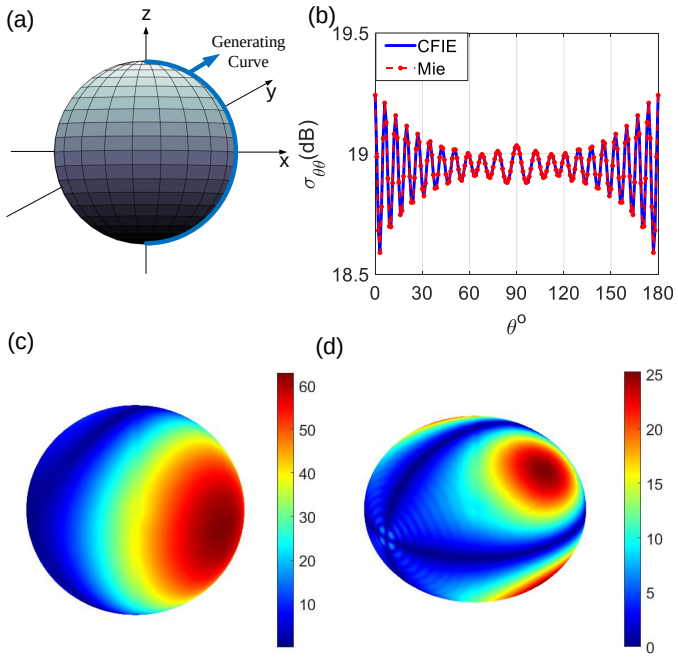

Fig. 7. Scattering analysis of a spherical PEC body of revolution having the radius of $r/\lambda = 5$ ($\lambda = 1$ is the normalized wavelength). The BOR is impinged by a plane wave incident field with the incident angle $\theta_i = \pi/2$ and $\phi_i = 0$. (b) $\sigma_{\theta\theta}$ in the plane $\phi_{obs} = 0$. The results are obtained from the proposed CFIE method (solid blue line) and compared with Mie series (dashed red line) [33]. The maximum deviation between the CFIE technique and the Mie series is 0.004 dB, (c) and (d) Three-dimensional distribution of the surface current densities (in absolute values) in the direction tangential to the generating curve (panel c) and in the ϕ direction.

B. Analysis of scattering by BORs using the CFIE

To illustrate the ability to compute the MGFs and the impedance matrices for a relatively large number of modes, while still having an analytical reference, we consider a spherical PEC scatterer with radius $r = 5\lambda$ in free space, illuminated by a θ-polarized plane wave with unit amplitude and incident angle $\theta_i = \pi/2$. Owing to the symmetry of the sphere, we can compare this case to the scattering by a normally incident plane wave with the Mie series for which only the modes $m = \pm 1$ are excited upon application of a transformation of coordinates. For the case $\theta_i = \pi/2$, the modes $m = -65, \ldots, 65$ are taken into account. The generating curve of the spherical BOR is discretized into 200 segments. The corresponding $\sigma_{\theta\theta}$ in the plane $\phi_{obs} = 0$ is shown in Fig. 7(b), computed using the proposed approach (blue line) for $\theta_i = \pi/2$. The obtained result agrees well with the solution from the Mie series [33], indicated by the dotted red line in Fig. 7(b). The maximum deviation between the CFIE technique and the Mie series is 0.004 dB in this case. Figs. 7(c) and (d) depict the absolute values of the surface current densities corresponding to tangential (panel c) and ϕ-direction (panel d).

Next, we consider the electromagnetic scattering by a PEC cone. The incident wave parameter is $\theta_i = \pi/4$. The radius r of the ground plane and the height h of the cone are specified by $r/\lambda = 0.8$ and $h/\lambda = 2$, respectively. The corresponding generating curve is discretized into 40 segments and Fourier modes $m = -20, \ldots, 20$ are taken into account to compute the RCS and the surface current densities on the cone surface. Fig. 8(a) shows the co-polarized components $\sigma_{\theta\theta}$ and $\sigma_{\phi\phi}$ of the RCS matrix for this scattering problem, obtained using the proposed CFIE approach. Fig. 8(c) and (d) show the absolute values of the surface current densities corresponding to the direction tangential to the generating curve and in the ϕ direction.

We also analysed the PEC cone scattering for normal incidence, $\theta_i = 0$, which was already investigated in [37]. Fig. 8(b) compares the corresponding $\sigma_{\theta\theta}$, obtained using the CFIE (blue curve) with the result from [37] (red dotted curve). The results are in good agreement, even though the method proposed in [37] is not based on BOR symmetry. The maximum deviation between the CFIE technique and the curve from the literature is 0.97 dB (maximum absolute difference between the two curves in Fig. 8(b)). As for the computational speed, the computation time of the proposed method was 213 s. On the other hand, based on the data provided in Table I of [37] and assuming that computation times scale linearly with the number of Rao–Wilton–Glisson (RWG) basis functions, extrapolation for the cone would take 538 s or 195 s when employing their MB-RWG or MB-RWG-BP approaches, respectively. Here, it should be noted that, while we used Matlab 2019b on a laptop with 16 GB of RAM and an Intel core i7-8850H processor for obtaining the results presented in Fig. 8(b), a different programming language and computer platform may have been employed in [37], which has a bearing on the comparison between the methods.

To demonstrate the benefit of the proposed acceleration method, we repeated the same computation without using the proposed acceleration scheme. The corresponding computation time was 412 s in the latter case. These results clearly indicate the benefits of the proposed acceleration method.

C. Computation of the MGFs for a large BOR

We conclude by considering the scattering analysis for a big axially symmetric parabolic reflector shown in Fig. 9(a), which requires the computation of many modes due to its large size. The corresponding generating curve (green curve in the figure) is plotted in Fig. 9(b). The frequency of operation is considered as $f = 30$ GHz. The geometrical parameters are $F_{\text{ref}} = 240\lambda$ (F_{ref} is the focal point of the parabolic reflector), $A_{\text{ref}} = 400\lambda$. The remaining parameter Z_{ref} can be computed as [38]

$$Z_{\text{ref}} = \frac{(A_{\text{ref}})^2}{4F_{\text{ref}}}. \tag{8}$$

To be able to employ the CFIE, the generating curve corresponding to the BOR must be closed or end on the axis of symmetry. To satisfy this criterion, the dashed green line shown in Fig. 9(b) is added to the parabolic section of the generating curve. For an obliquely incident plane wave with angle of incidence $\theta_i = \pi/4$, at least 3821 ($m = -1910, \ldots, 1910$) modes are required to represent the plane wave in terms of Bessel functions on the domain of the reflector with accuracy up to machine precision. The generating curve is discretized

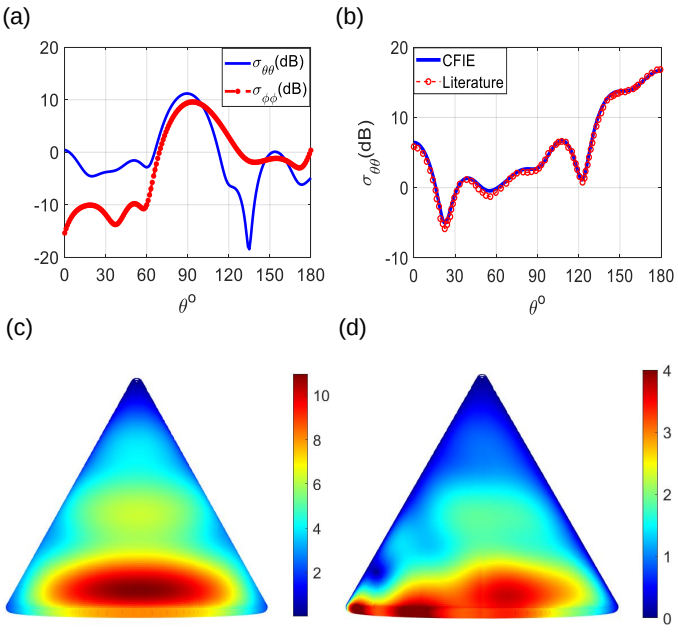

Fig. 8. Scattering analysis of a cone-like PEC body of revolution having with the radius of $r/\lambda = 0.8$ and the height of $h/\lambda = 2$. (a) $\sigma_{\theta\theta}$ and $\sigma_{\phi\phi}$ of component of the bistatic radar cross-section in the plane $\phi_{obs} = 0$, corresponding to the $\theta_i = \pi/4$ (b) $\theta\theta$ component of the bistatic radar cross-section at the plane $\phi_{obs} = 0$, computed from the proposed CFIE method (solid blue curve) and from [37] (dashed red curve). The results are computed for a normally incident plane wave. The maximum deviation between the CFIE technique and the curve from the literature is 0.97 dB, (c) and (d) Three-dimensional distribution of the surface current densities in the direction tangential to the generating curve (panel c) and in the ϕ direction (panel d).

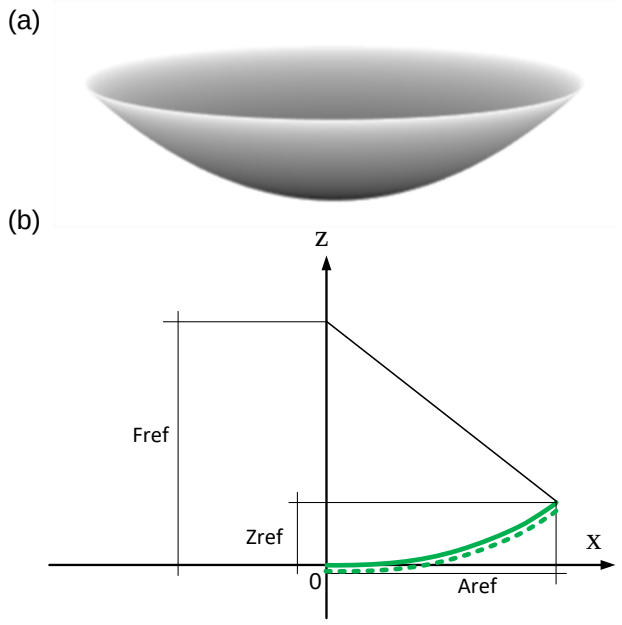

Fig. 9. (a) Parabolic reflector antenna. (b) The corresponding generating curve.

with 80 segments. The computation of the starting and end values g_0, g_1, g_{1909}, and g_{1910} is performed by Matlab's `integral` routine with an absolute error below 10^{-15}. The two end values are only computed for $w > 0.99$, which amounts to 17% of all possible values for w. All other MGFs from $m = 2$ to $m = 1908$ are computed using the penta-diagonal matrix system.

While the parabolic reflector antenna under investigation does not have an interior resonance for the selected frequency, our main goal here is to demonstrate the applicability of the proposed method when a large number of modes is required. In Table II, the computational characteristics of the problem under investigation are summarized. From the table we observe that the initialization time is significant but not dominant when so many modes are taken into account. In addition, the computation of the MFIE starting and end values takes more time than the EFIE case. The table also includes information regarding the accuracy of the computation of the corresponding MGFs. As a representative example mentioned in the last row, the maximum absolute error of MGF for $m = 1000$ was 4.21×10^{-9} and 7.36×10^{-9} for the EFIE and MFIE, respectively. Another conclusion from Table II is that, for the intermediate modes ($m = 2$ to $m = 1908$), the computation time of the MGFs using penta-diagonal matrix, is two order of magnitudes shorter than the Matlab's `integral` routine for the EFIE and MFIE cases, respectively.

Next, by employing the CFIE technique, the scattered electric field from the induced current over the BOR is computed in the focal plane of the parabolic reflector, i.e. $z = F_{\text{ref}}$. To this end, we gradually change the incident angle from $\theta_i = 0°$ to $\theta_i = 45°$, and evaluate the corresponding scattered electric field at the focal plane. We assume that the reflector is illuminated with a θ-polarized plane wave with unit amplitude. Fig. 10 represents the absolute value of the scattered electric field ($|\mathbf{E}^s|$) at the so-called focal plane of the reflector for different values of the incident angle, namely $\theta_i = 0°, 2°, 20°$, and $45°$. As observed for $\theta_i = 0°$, the maximum of $|\mathbf{E}^s|$ occurs at the focal point of the parabolic reflector (panel a). For normal incidence, the two excitation vectors $\mathbf{V}_{EFIE}$ and $\mathbf{V}_{MFIE}$ are only non-zero for modes $m = \pm 1$. However, for obliquely incident plane waves, the excitation vectors are non-zero and become significant for more modes. For instance, at $\theta_i = 2°$, the excitation vector elements are greater than machine precision for $m = -140, \ldots, 140$. For larger θ_i more modes contribute, e.g., for $\theta_i = 20°$ and $\theta_i = 45°$, $m = -960, \ldots, 960$, and $m = -1910, \ldots, 1910$ must be considered, respectively. As expected, the maximum of $|\mathbf{E}^s|$ shifts away from the focal point as the incident angle θ_i increases.

V. Conclusion

We investigated the computation of the MGFs arising in the EFIE and MFIE in a direct manner using five-term recurrence relations. The maximum absolute error in computing the MGFs through the recurrence relations was 10^{-13}. The direct nature of the proposed formulation is advantageous in scattering problems by large BORs, involving many Fourier modes.

TABLE II
COMPUTATIONAL CHARACTERISTICS OF SCATTERING OF PEC PARABOLIC REFLECTOR FOR THE MAXIMUM NUMBER OF MODES PERTAINING TO THE CASE WITH THE INCIDENT ANGLE PARAMETERS OF $\theta_i = \pi/4$, $\phi_i = 0$.

Definition	EFIE	MFIE
Number of modes	1910	1910
Number of segments	80	80
The number of MGF evaluations per mode	158200	158200
Computation time of the starting and end values required for penta-diagonal matrix (the first and last two MGFs)	11m : 02s	16m : 21s
Initialization time and computation time of inverse of penta-diagonal matrix system	$04h : 32m$	$04h : 47m$
Maximum error of computing MGF for mode $m = 1000$	4.21×10^{-9}	7.36×10^{-9}

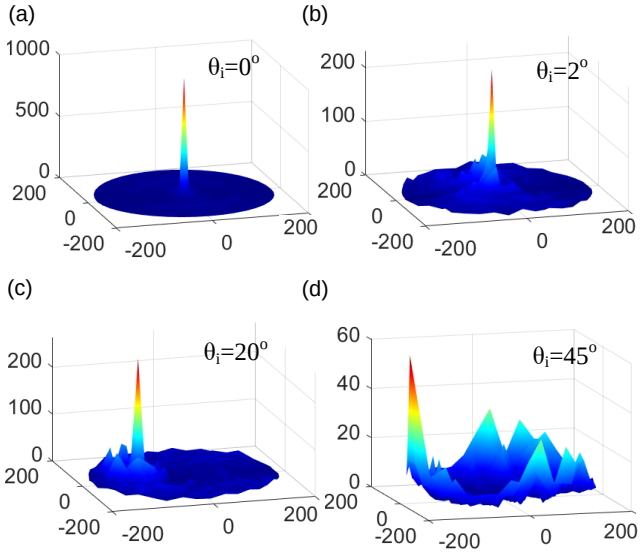

Fig. 10. Absolute value of the scattered electric field in the focal plane of parabolic reflector for (a) $\theta_i = 0°$, (b) $\theta_i = 2°$, (c) $\theta_i = 20°$, and (d) $\theta_i = 45°$. The results are obtained from the proposed CFIE technique. The horizontal axes are the distance in centimeters from the focal point.

For relatively large parabolic reflector, we have shown that the computation time of the MGFs using the proposed method is shorter than Matlab's `integral` routine by two orders of magnitudes. To overcome interior resonance problems, the EFIE and MFIE were combined in a CFIE formulation for BORs.

ACKNOWLEDGMENT

This research was supported by the NWO-TTW HTSM project MAX META-XT, under project number 16184.

APPENDIX A

In this section, we discuss the derivation of the five-term recurrence relation of the MFIE MGF. We start by reiterating the MFIE MGF,

$$g_m^H = \int_0^\pi \cos(m\alpha)(1 + jk_0R(\alpha))\frac{e^{-jk_0R(\alpha)}}{R^3(\alpha)}d\alpha. \quad (9)$$

By using the parameter w defined in the text and defining a new parameter $\alpha' = \frac{\alpha-\pi}{2}$, g_m^H can be re-expressed as

$$g_m^H = 2(-1)^m(\frac{w}{4\rho\rho'})^{3/2}\int_0^{\pi/2}\cos(2m\alpha)G_{w,k'}^H(\alpha)d\alpha, \quad (10)$$

in which

$$G_{w,k'}^H(\alpha) = (1+jk'\sqrt{1-w\sin^2\alpha})\frac{e^{-jk'\sqrt{1-w\sin^2\alpha}}}{(1-w\sin^2\alpha)^{3/2}}. \quad (11)$$

Considering the following well-known relation

$$\begin{aligned}\cos(2m\phi) =&2(1-2\sin^2\phi)\cos(2(m-1)\phi)\\ &-\cos(2(m-2)\phi),\end{aligned} \quad (12)$$

the following relation can be obtained for g_m^H

$$\begin{aligned}g_m^H(w,k') =& -2g_{m-1}^H(w,k') - g_{m-2}^H(w,k')\\ &-\frac{4}{w}I_{m-1}^H + \frac{4}{w}g_{m-1}^H,\end{aligned} \quad (13)$$

for which we have

$$\begin{aligned}I_m^H(w,k') =& 2(-1)^m(\frac{w}{4\rho\rho'})^{3/2}\\ &\int_0^{\pi/2}\cos(2m\alpha)(1-w\sin^2\alpha)G_{w,k'}^H(\alpha)d\alpha.\end{aligned} \quad (14)$$

For $m \neq 0$, by using the integration by parts method, I_m can be written as

$$\begin{aligned}I_m^H(w,k') =&\frac{w}{8m}\left[g_{m-1}^H(w,k') - g_{m+1}^H(w,k')\right]\\ &+k'^2\frac{w}{8m}\left[J_{m-1}^H(w,k') - J_{m+1}^H(w,k')\right],\end{aligned} \quad (15)$$

where,

$$\begin{aligned}J_m^H(w,k') =&2(-1)^m(\frac{w}{4\rho\rho'})^{3/2}\\ &\int_0^{\pi/2}\cos(2m\alpha)\frac{e^{-jk'\sqrt{1-w\sin^2\alpha}}}{\sqrt{1-w\sin^2\alpha}}d\alpha.\end{aligned} \quad (16)$$

Likewise, applying integration by parts to $J_m^H(w)$ yields

$$J_m^H(w,k') = \frac{w}{8m}\left[g_{m-1}^H(w,k') - g_{m+1}^H(w,k')\right]. \quad (17)$$

Substituting (17) and (15) in (13) leads to the five-term recurrence relation in (3).

REFERENCES

[1] M. Andreasen, "Scattering from bodies of revolution," *IEEE Transactions on Antennas and Propagation*, vol. 13, no. 2, pp. 303–310, 1965.
[2] J. R. Mautz and R. Harrington, "Radiation and scattering from bodies of revolution," *Applied Scientific Research*, vol. 20, no. 1, pp. 405–435, 1969.
[3] A. W. Glisson and D. R. Wilton, "Simple and efficient numerical techniques for treating bodies of revolution," MISSISSIPPI UNIV UNIVERSITY, Tech. Rep., 1979.
[4] S. M. A. Hamed and S. Bashir, "New exact series for modal Green's function," in *2015 International Conference on Computing, Control, Networking, Electronics and Embedded Systems Engineering (ICCNEEE)*. IEEE, 2015, pp. 83–86.
[5] J. Lai and M. O'Neil, "A fast and high order algorithm for the electromagnetic scattering of axis-symmetric objects," in *2018 IEEE International Conference on Computational Electromagnetics (ICCEM)*. IEEE, 2018, pp. 1–2.

[6] C. L. Epstein, L. Greengard, and M. O'Neil, "A high-order wideband direct solver for electromagnetic scattering from bodies of revolution," *Journal of Computational Physics*, vol. 387, pp. 205–229, 2019. [Online]. Available: https://www.sciencedirect.com/science/article/pii/S0021999119301585

[7] F. Sepehripour, B. P. de Hon, and M. C. van Beurden, "Enhancing the computational speed of the modal Green function for the electric-field integral equation for a body of revolution," in *Scientific Computing in Electrical Engineering, SCEE 2022*, 2022.

[8] S. Gedney and R. Mittra, "The use of the FFT for the efficient solution of the problem of electromagnetic scattering by a body of revolution," in *1988 IEEE AP-S. International Symposium, Antennas and Propagation*. IEEE, 1988, pp. 92–95.

[9] A. Abdelmageed, "Efficient evaluation of modal Green's functions arising in EM scattering by bodies of revolution," *Progress In Electromagnetics Research*, vol. 27, pp. 337–356, 2000.

[10] A. A. Mohsen and A. K. Abdelmageed, "A fast algorithm for treating EM scattering by bodies of revolution," *AEU-International Journal of Electronics and Communications*, vol. 55, no. 3, pp. 164–170, 2001.

[11] W. M. Yu, T. J. Cui, *et al.*, "Closed form modal Green's functions for accelerated computation of bodies of revolution," *IEEE Transactions on Antennas and Propagation*, vol. 56, no. 11, pp. 3452–3461, 2008.

[12] J. Vaessen, "Efficient modeling of electromagnetic fields in stochastic configurations," Ph.D. dissertation, Technische Universiteit Eindhoven, 2015.

[13] F. Sepehripour, M. C. van Beurden, and B. P. de Hon, "An error analysis of the three-term recurrence relation of the modal Green function," in *2022 International Conference on Electromagnetics in Advanced Applications (ICEAA)*, 2022, pp. 070–070.

[14] J. L. Schmitz, "Efficient solution for electromagnetic scattering using the dual-surface magnetic-field integral equation for bodies of revolution," in *Proceedings of IEEE Antennas and Propagation Society International Symposium and URSI National Radio Science Meeting*, vol. 3. IEEE, 1994, pp. 2318–2321.

[15] A. A. Mohsen and A. K. Abdelmageed, "Magnetic field integral equation for electromagnetic scattering by conducting bodies of revolution in layered media," *Progress In Electromagnetics Research*, vol. 24, pp. 19–37, 1999.

[16] W. D. Wood, A. W. Wood, and J. L. Fleming, "EM scattering from bodies of revolution using the locally corrected nystro/spl uml/m method," in *IEEE Antennas and Propagation Society Symposium, 2004.*, vol. 4. IEEE, 2004, pp. 4036–4039.

[17] Ú. C. Resende, F. J. Moreira, and O. M. Pereira-Filho, "Efficient evaluation of singular integral equations in moment method analysis of bodies of revolution," *Journal of Microwaves, Optoelectronics and Electromagnetic Applications (JMOe)*, vol. 6, no. 2, pp. 373–391, 2007.

[18] W. C. Gibson, *The method of moments in electromagnetics*. CRC press, 2014.

[19] F. Sepehripour and M. C. van Beurden, "Accurate and efficient evaluation of the scattering of bodies of revolution based on magnetic field integral equation," *Progress in Electromagnetics Research M*, vol. 108, pp. 1–15, 2022.

[20] P. Bolli, G. G. Gentili, R. Nesti, and G. Pelosi, "Coupled BORs scattering via an efficient MoM solution of CFIE," *Microwave and Optical Technology Letters*, vol. 37, no. 3, pp. 180–183, 2003.

[21] M. Li, Y. Hu, R. Chen, and G. Vecchi, "Electromagnetic modeling of moving mixed conductive and dielectric bors with an effective domain decomposition method," *IEEE Transactions on Antennas and Propagation*, vol. 68, no. 12, pp. 7978–7985, 2020.

[22] Q. Zhou, L. Wang, M. Li, and R. Chen, "Effective modeling of seperating body of revolution targets with domain decomposition method," in *2020 International Conference on Microwave and Millimeter Wave Technology (ICMMT)*. IEEE, 2020, pp. 1–2.

[23] M. Nasirian, M. Maddahali, M. Maddah-Ali, A. Bakhtafrouz, and M. H. Sadrearhami, "CFIE-based DDM with full exploitation of BoR basis for scattering from compound BoR-and-Non-BoR PEC object," *IEEE Transactions on Antennas and Propagation*, vol. 70, no. 1, pp. 773–776, 2021.

[24] S. D. Gedney and R. Mittra, "The use of the FFT for the efficient solution of the problem of electromagnetic scattering by a body of revolution," *IEEE Transactions on Antennas and Propagation*, vol. 38, no. 3, pp. 313–322, 1990.

[25] J. L. Fleming, A. W. Wood, and W. D. Wood Jr, "Locally corrected nyström method for EM scattering by bodies of revolution," *Journal of Computational Physics*, vol. 196, no. 1, pp. 41–52, 2004.

[26] J. A. H. M. Vaessen, M. C. van Beurden, and A. G. Tijhuis, "Accurate and efficient computation of the modal Green's function arising in the electric-field integral equation for a body of revolution," *IEEE Transactions on Antennas and Propagation*, vol. 60, no. 7, pp. 3294–3304, 2012.

[27] F. Sepehripour, M. C. van Beurden, and B. P. de Hon, "Direct computation of the PEC body of revolution modal Green function for the electric field integral equation," *IEEE Journal on Multiscale and Multiphysics Computational Techniques*, vol. 7, pp. 186–194, 2022.

[28] O. Bucci and G. Franceschetti, "On the spatial bandwidth of scattered fields," *IEEE Transactions on Antennas and Propagation*, vol. 35, no. 12, pp. 1445–1455, 1987.

[29] O. M. Bucci and G. Franceschetti, "On the degrees of freedom of scattered fields," *IEEE Transactions on Antennas and Propagation*, vol. 37, no. 7, pp. 918–926, 1989.

[30] J. T. Kelley, A. Yilmaz, and Y. Brick, "Robust grid-based computation of Hmatrix blocks' low-rank approximation for vector basis functions," *IEEE Transactions on Antennas and Propagation*, 2022.

[31] D. Zvulun, Y. Brick, and A. Boag, "A generalized source integral equation for enhanced compression in three dimensions," *IEEE Transactions on Antennas and Propagation*, 2023.

[32] J. T. Kelley, A. E. Yılmaz, and Y. Brick, "An iterative random sampling algorithm for rapid and scalable estimation of matrix spectra," *IEEE Journal on Multiscale and Multiphysics Computational Techniques*, vol. 8, pp. 205–216, 2023.

[33] Giannakopoulos, Ilias, "Matlab software for the Mie scattering of PEC and homogeneous spheres irradiated by a linearly polarized plane wave," 2018. [Online]. Available: https://www.github.com/GiannakopoulosIlias/MieScattering

[34] J. A. Stratton, *Electromagnetic Theory*, 1st ed. McGraw-Hill Companies (New York), 1941.

[35] C. A. Balanis, *Advanced engineering electromagnetics*. John Wiley & Sons, 2012.

[36] J. Lappalainen, P. Ylä-Oijala, D. C. Tzarouchis, and A. Sihvola, "Resonances of characteristic modes for perfectly conducting objects," *IEEE Transactions on Antennas and Propagation*, vol. 65, no. 10, pp. 5332–5339, 2017.

[37] S. Huang, G. Xiao, Y. Hu, R. Liu, and J. Mao, "Multibranch Rao–Wilton–Glisson basis functions for electromagnetic scattering problems," *IEEE Transactions on Antennas and Propagation*, vol. 69, no. 10, pp. 6624–6634, 2021.

[38] J. Wang, J. xiang Ge, Y. Zhou, H. Xia, and X. zhi Yang, "Design of a high-isolation 35/94-GHz dual-frequency orthogonal-polarization Cassegrain antenna," *IEEE Antennas and Wireless Propagation Letters*, vol. 16, pp. 1297–1300, 2016.